Biomacromolecules

ACS AuthorChoice

Article

pubs.acs.org/Biomac

Terms of Use

Synthetic Oral Mucin Mimic from Polymer Micelle Networks

Sundar P. Authimoolam,[†] Andrew L. Vasilakes,[†] Nihar M. Shah,[†,‡] David A. Puleo,[§] and Thomas D. Dziubla*[,†]

[†]Department of Chemical and Materials Engineering, College of Engineering, University of Kentucky, 177 F. Paul Anderson Tower, Lexington, Kentucky 40506, United States

[§]Department of Biomedical Engineering, College of Engineering, University of Kentucky, Wenner-Gren Laboratory, Lexington, Kentucky 40506, United States

Supporting Information

ABSTRACT: Mucin networks are formed in the oral cavity by complexation of glycoproteins with other salivary proteins, yielding a hydrated lubricating barrier. The function of these networks is linked to their structural, chemical, and mechanical properties. Yet, as these properties are interdependent, it is difficult to tease out their relative importance. Here, we demonstrate the ability to recreate the fibrous like network through a series of complementary rinses of polymeric worm-like micelles, resulting in a 3-dimensional (3D) porous network that can be deposited layer-by-layer onto any surface. In this work, stability, structure, and microbial capture capabilities were evaluated as a function of network properties. It was found that network structure alone was sufficient for bacterial capture, even with networks composed of the adhesion-resistant polymer, poly(ethylene glycol). The synthetic networks provide an excellent, yet simple, means of independently characterizing mucin network properties (e.g., surface chemistry, stiffness, and pore size).

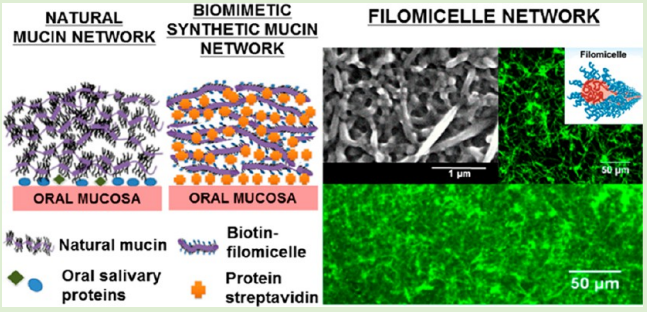

INTRODUCTION

Amphiphilic di- and triblock copolymers capable of generating complex micelles (e.g., filamentous micelles, spherical micelles, vesicles, and lamellae) have received significant attention given their potential use in biomedical applications.[1−4] More recently, these preassembled nanoscale systems have been shown to serve as building blocks in layer-by-layer (LBL) systems, yielding even more complex hierarchical superstructures.[5,6] The ability of these complex superstructures to incorporate protected drug cargo and form bioactive surfaces has generated interest in drug delivery[7] and biomimetic application.[8−10]

By taking cues from oral biology, it may be possible to use directed self-assembly of such systems to easily recreate the micro/nanoscale features of mucin networks. In the oral cavity, natural mucin serves a multitude of functions to ensure oral health, which include providing a lubricating barrier, maintaining surface hydration, and acting as a sacrificial trap for debris and bacteria to protect the underlying tissue.[11,12] At the molecular level, mucins are filamentous glycoproteins, with a "bottle-brush" like structure.[11,13,14] They self-associate via disulfide linkages to form longer brushes (mucin multimers). Upon further higher order associations, these multimers form a multilayered film, which is a complex 3-dimensional (3D) mucin network with pores ranging in size from nanometers to microns.[15,16] This complexation is facilitated by wide variety of molecular interactions such as disulfide bridging, hydrophobic, electrostatic forces and hydrogen bonding.[8] Due to such formation complexity, these networks pose a significant challenge to researchers in understanding its structure, biofunction and its biogenesis.[9] Also, when the soft buccal tissues lack this mucin barrier, a perception of dryness followed by painful inflammation (e.g., xerostomia) can develop.[17] This loss of barrier protection and lubricity increases the susceptibility to infections, dental caries, and mucosal ulceration. Patients with more severe cases may even experience a difficulty to perform routine oral activities, such as chewing and swallowing, leading to dysphasia.[12]

In this work, a simple biomimetic system that can recreate the mucin network is presented (Scheme 1). Polymeric micelles[3,18,19] were deposited onto a surface in a series of alternating rinses of complementary cross-linking chemistries. Through control of the shape/structure of the micelles (e.g., filomicelles or spherical micelles), it was possible to generate a 3-dimensional network structure similar to that of natural mucin. As a proof of concept, biotinylated polymeric micelles were deposited as layer-by-layer (LBL) via biotin−streptavidin affinity interactions. We demonstrate the impact of micelle structure and number of layer additions (NoL) on network stability and morphology. The NoL indicates the number of micelle additions cycles performed during the LBL deposition

Received: May 13, 2014
Revised: July 2, 2014
Published: July 3, 2014

Scheme 1. Simplified Illustration Comparing the Formation of the Proposed Polymeric Micelle-LBL Network as a Synthetic Oral Mucin Mimic to That of Naturally Occurring Oral Mucin Network

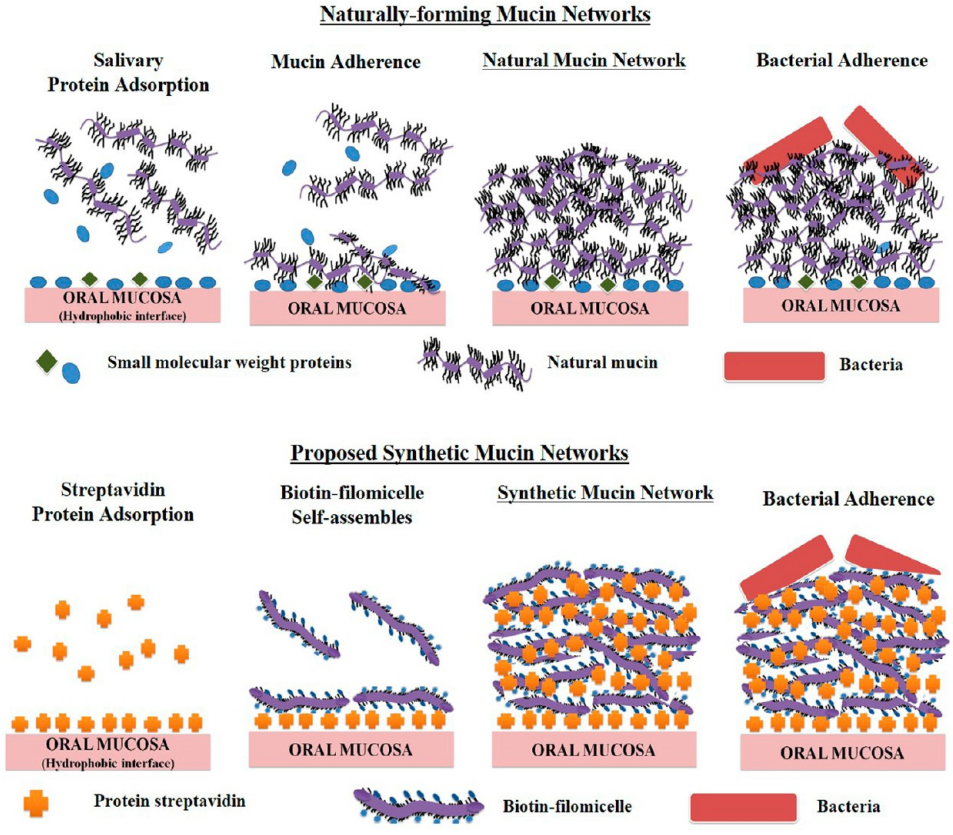

process. Further, it was shown that, although the micelles were composed of dense antiadhesive PEG polymers, the filomicelle 3D network structure was able to recreate the bacterial capture capability of mucin networks. These synthetic mucin networks can potentially serve as a modular in vitro model in studying *trans*-mucosal drug delivery. With careful selection of building blocks, the network properties can be tailored to decouple its charge, porosity, and thickness effects on drug (nanoparticle) permeation across networks.[20,21] Analogously, those network properties (structural and functional) can be extended to provide a more fundamental understanding of mucin-bacterial interactions (e.g., charge vs structural properties of the mucin network resulting in bacterial capture).

In the current study, micelle networks were evaluated for their physical network properties (e.g., morphology, thickness, network-pore size, and growth mechanism) to determine their ability to recapitulate the fibrous networks of natural mucin systems.[22−26] Thus, the theme of this work was to recreate the physical mucin-like structure without changing the chemical properties. We expect the surface chemistry of these micelles can also be independently modified to alter their chemical properties (e.g., adhesiveness, affinity, selectivity), suggesting that these networks represent an interesting tool for decoupling chemistry and morphology when identifying mucin network functionality.

EXPERIMENTAL SECTION

Materials. 3,6-Dimethyl-1,4-dioxane-2,5-dione (lactide), poly(ethylene glycol) methyl ether (molecular weight (MW) ∼ 5000 Da), stannous 2-ethylhexanoate, curcumin (from curcuma longa), protease derived from *Streptomyces griseus* (pronase), 2-(4-hydroxyphenylazo) benzoic acid (HABA), nile red, anhydrous diethyl ether, glucose, and crystal violet were purchased from Sigma-Aldrich (St. Louis, MO). Biotin-poly(ethylene glycol)amine was purchased from Laysan Bio, Inc. (Arab, AL). Poly(D,L-lactide) (acid terminated; inherent viscosity 0.15−0.25 dL/g) was purchased from Durect (Cupertino, CA). Recombinant streptavidin (produced in *E. coli*) was purchased from Prospec-Tany (East Brunswick, NJ). Avidin (from egg whites) was purchased from Life Technologies (Grand Island, NY). Chloroform, *N*,*N*′-dicyclohexylcarbodiimide (DCC), and dichloromethane (DCM) were purchased from Acros Organics (Waltham, MA). Dimethyl sulfoxide was purchased from Fisher Scientific (Pittsburgh, PA). Iodogen iodination reagent (1,3,4,6-tetrachloro-3α-6α-diphenylglycouril) was purchased from Thermo Scientific (Rockfort, IL). *Staphylococcus aureus* subspecies Rosenbach was purchased from ATCC (Manassas, VA).

Rat dermal tissue was prepared by excising the dorsal skin flap (thoracic to abdominal area) of a freshly euthanized rat. The harvested tissue was placed in a saline soaked towel and stored in an airtight polyethylene ziplock bag at −80 °C. The tissue was thawed to room temperature prior to use.

Biotin-Functionalized Polymeric Micelle (Biotin-Micelle) Synthesis. Biotin-micelles were synthesized using a previously described cosolvent/evaporation method.[27] Blends of custom-synthesized poly(ethylene glycol)-*b*-poly(lactic acid) (PEG-*b*-PLA) based diblock copolymers, methoxy-PEG-PLA (50 mg, ∼91% w/w) and biotinylated-PEG-PLA (5 mg, ∼9% w/w; see Supporting Information and Figures S1 and S2 for diblock copolymer synthesis and characterization) were dissolved in a water-immiscible organic solvent (chloroform), which was then dispersed in a continuous aqueous phase (deionized (DI) water, 50 mL) using an ultrasonic homogenizer (Fisher Scientific, Sonic dismembrator Model 100). The oil/water dispersion was vigorously stirred overnight (∼16 h) at room temperature until the organic solvent was completely evaporated off to form hardened biotin-micelles.[28] Micelles were visualized by adding

dx.doi.org/10.1021/bm5006917 | *Biomacromolecules* 2014, 15, 3099−3111

nile red stain (0.05 mg, ~0.09% w/w) or curcumin (1.5 mg, ~2.65% w/w) during synthesis.

Upon hardening, the biotin-micelles were centrifuged (1000 rpm for 10 min) to separate larger sized macroparticles from the desired micelle fraction. The micelle fraction was again centrifuged (7500 rpm for 45 min) and resuspended in DI water to remove excess curcumin or nile red stain. Micelles without biotin were synthesized using a similar procedure but using mPEG-PLA without adding biotin-PEG-PLA polymer during formulation.

Formation of Layer-by-Layer Networks of Micelle (Micelle-LBL). In vitro micelle-LBL networks were deposited on biotin-coated plates (Thermo Scientific Pierce, Rockford, IL, preblocked 96-well strip plates) at room temperature. The base biotin layer was alternatively rinsed with streptavidin (1 mg/mL in phosphate buffered saline (PBS, pH 7.4), 100 μL/well, and 1 min incubation) and micelles (~5 mg/mL in DI water, 100 μL/well, and 1 min incubation). To develop and verify the ability to deposit LBL networks via biotin−streptavidin interactions, networks were developed using biotinylated-micelles (spherical micelles (SM) and filamentous micelles (FM)) and micelles without biotin separately. Excess micelles and streptavidin during LBL deposition were removed with PBS rinses between each layer. To demonstrate the micelle-LBL (FM-LBL or SM-LBL networks) growth, networks with an increasing number of layer additions (NoL = 1, 3, 5, and 7) were developed. In order to quantify and visualize the developed LBL networks, the fluorophore curcumin was loaded into the micellar cores. The homogeneity of micelle-LBL network deposition on the entire base surface was mapped using fluorescence (from curcumin) area scans using a microplate spectrophotometer (Ex/Em: 420/500 nm, top/bottom read, BioTek Synergy Mx, Gen5 2.0, Winooski, VT). To visualize the micelle-LBL networks (FM-LBL and SM-LBL networks) using epifluorescence microscopy (Nikon Eclipse LV100, FITC filter, under 10×/20×/50× objectives, NIS Elements), networks were deposited on larger diameter streptavidin adsorbed polystyrene 12-well microplates at room temperature under similar conditions.

Evaluating FM-LBL Network Thickness. FM-LBL networks were developed on streptavidin-adsorbed glass bottom culture-dishes adopting the same procedure as described above under micelle-LBL network formation. Preliminary visualization of network growth was carried out using confocal laser scanning microscopy (Leica TSP SP5 Confocal, Leica Microsystems, UV Laser (405 Diode), GFP filter, under a 63× water objective). Optical sectioning was carried out along the $x-y$ plane to generate z-stack images for evaluating the degree of heterogeneity within each sample prior to thickness measurement (Figure S5 in Supporting Information). Upon visual verification of LBL network formation and homogeneity, its thickness was determined by optical sectioning along the transverse $x-z$ planes to generate y-stack (cross-sectional) images. Throughout the imaging process, the samples were kept immersed in water to eliminate refractive index differences in the optical medium.

Scanning Electron Microscopy of Micelle-LBL Networks. SM or FM-LBL networks with different number of layer additions (NoL = 1, 3, 5, and 7) were deposited on a polystyrene substrate adopting the same procedure described above under micelle-LBL networks formation. Excess micelles and streptavidin were removed by PBS rinses between each layer and finally rinsed off with DI water (0.2 μm filtered) post-network development. The micelle-LBL networks were visualized under a scanning electron microscope (SEM, S-4300, Hitachi), and images were taken at randomly selected locations at different magnifications.

Ex Vivo FM-LBL Network Formation. Rat dermal tissues (circular patches of diameter ~ 15 mm) excised from freshly euthanized rats were used as an ex vivo model for the human mucosal surface. With the epidermal side placed face-down, the FM-LBL network was deposited on the exposed dermal surface. First, a base streptavidin layer was deposited (1 mg/mL in PBS, 100 μL/well, 2 min incubation). This was followed by alternating rinses of FM (~10 mg/mL in DI water, 100 μL/well, 1 min incubation) and streptavidin (1 mg/mL in PBS, 100 μL/well, 1 min incubation) until a desired NoL (1, 3, 5, 7) were deposited. FM (biotin-FM and FM-without biotin) was used separately during LBL deposition to verify the ex vivo formation of FM-LBL networks. Excess FM and streptavidin were removed by rinses with PBS between each layer. Tissues coated with FM-LBL networks were placed inside cells of a 12-well plate and network growth was determined using fluorescence (from curcumin) using a microplate spectrophotometer (Ex/Em: 420/500 nm, top/bottom read, BioTek Synergy Mx, Gen5 2.0, Winooski, VT). Tissues coated with FM-LBL networks (NoL = 7) containing either biotin-FM or equivalent control (FM without biotin) were also imaged using epifluorescence microscopy.

Streptavidin Destabilization from FM-LBL Networks. FM-LBL networks were developed using a modified micelle-LBL network formation procedure, described below. FM-LBL network destabilization was studied by tracking loss of radiolabeled streptavidin (^{125}I-streptavidin) from the network interlayers and from the lower-most streptavidin layer independently (procedure for streptavidin radiolabeling is detailed in Supporting Information).

For measuring the network interlayers, a nonradiolabeled streptavidin layer was first added to the base biotin layer, followed by alternating biotin-FM and ^{125}I-streptavidin additions until the desired NoL (=7) were deposited. For measuring the lower-most layer, a similar procedure was adopted, except that ^{125}I-streptavidin was added to the base biotin layer, while the overlaying layers were deposited using nonradiolabeled streptavidin. Networks were incubated in simulated saliva (100 μL of 1.3 mM KH_2PO_4, 16 mM Na_2HPO_4, 136.9 mM NaCl, pH = 6.75),[29] or pronase (0.01% w/v, 100 μL) at 37 °C for different durations. Streptavidin mass remaining in the FM-LBL networks was measured using a γ-counter (PerkinElmer 2470 Wizard^2).

Wettability Measurement. FM-LBL networks with different NoL (1, 3, 5, 7) were deposited on a polystyrene substrate. A sessile drop was microsyringed onto FM-LBL networks and on an unmodified polystyrene substrate (without FM-LBL network). The contact angle was measured using a goniometer (ramé-hart model 100, Drop image software, Succasunna, NJ), and the sessile drop was imaged to provide visual proof of the change in surface wettability.

Bacterial Growth on LBL Networks. SM-LBL and FM-LBL networks (NoL = 7, 10, and 14) were deposited onto PS microplates using micelles (biotin-SM or biotin-FM) without curcumin loading. To study the effect of drug on bacterial growth, micelles with curcumin loaded in their core were used. Curcumin-loaded SM-LBL and FM-LBL networks (NoL = 7) were deposited onto PS microplates. Note that 48-well tissue culture treated polystyrene plates (Becton Dickinson Biosciences, San Jose, CA) were used for all bacterial studies. The protocol used for bacterial growth and quantification was adopted from Merritt et al.[30] *Staphylococcus aureus* Rosenbach strain (ATCC 25923, Manassas, VA) were cultured overnight in liquid BD Bacto Brain Heart Infusion (BHI) broth. To evaluate growth on the LBL networks an additional 1% w/v D-glucose and 2% w/v sodium chloride were added to the BHI broth to enhance biofilm growth. The overnight culture (*S. aureus* in BHI media) was diluted in BHI medium to a workable optical density (0.5 OD at 600 nm) for cell-counting, then to a working concentration of 10^5 cell forming units (CFU)/200 μL. A total of 200 μL of culture suspension were added onto control substrate (without any LBL network) and onto the SM-LBL and FM-LBL networks and incubated at 37 °C for 24 h to allow bacterial growth.

Bacterial Growth Quantification Using Crystal Violet Assay. A 0.1% w/v crystal violet solution was prepared in DI water, and 40 μL were added to each well of the 48-well plates after bacterial growth for 24 h. After 10 min at room temperature, the supernatant was removed, and the substrates were washed with PBS three times. Acetic acid (200 μL, 30% v/v) was added and incubated for 10 min at room temperature to dissolve the crystal violet bound to the bacterial cell walls. The solution was then mixed using a pipet, and optical absorbance (Abs) values were measured using a spectrophotometer (BioTek Synergy Mx, Gen5 2.0, Winooski, VT) at λ = 600 nm. The bacterial growth on the LBL networks was calculated as a percentage of bacteria on the untreated control substrate using the following equation:

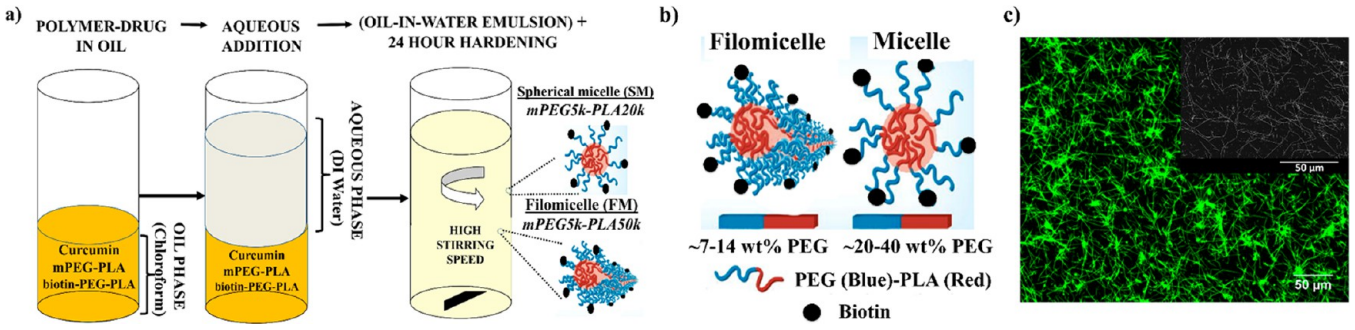

Figure 1. Polymeric micelles synthesized using mPEG-PLA diblock amphiphilic copolymers. (a) Scheme showing synthesis of biotin-micelles using the cosolvent/evaporation method. (b) Differences in copolymer amphiphilicity results in either spherical (SM) or filamentous (FM) micelle nanostructure morphology. (c) Visualization of curcumin loaded biotin-FM using fluorescence microscopy and scanning electron microscopy (inset).

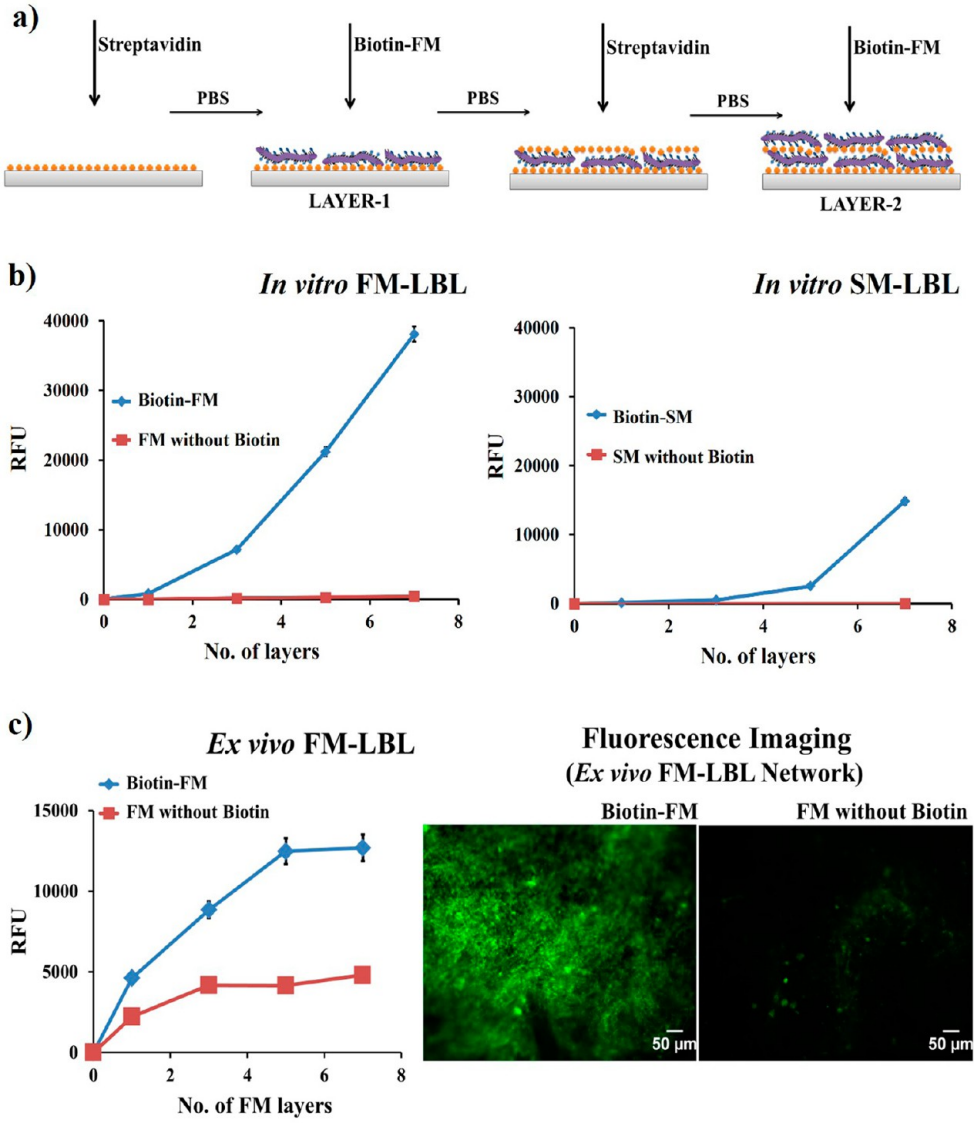

Figure 2. Formation of layer-by-layer networks of micelle (micelle-LBL). Micelle-LBL network growth was studied by tracking the relative fluorescence intensity (RFU) from curcumin-loaded micelles for increasing number of layer addition cycles (NoL). (a) Scheme showing formation of layer-by-layer networks of filomicelle (FM-LBL) using biotin−streptavidin affinity linkages by alternating additions of biotinylated-filomicelle (biotin-FM) and the protein streptavidin. Similarly, layer-by-layer networks of spherical micelle (SM-LBL) are formed from biotinylated-spherical micelle (biotin-SM) and the protein streptavidin (scheme not shown). (b) Micelle-LBL network growth using filomicelle (FM-LBL) and spherical micelle (SM-LBL). (c) Ex vivo FM-LBL network deposited on rat dermal tissue and visualized seven-layered FM-LBL networks through epi-fluorescence microscopy. FM without biotin did not result in network formation.

dx.doi.org/10.1021/bm5006917 | Biomacromolecules 2014, 15, 3099−3111

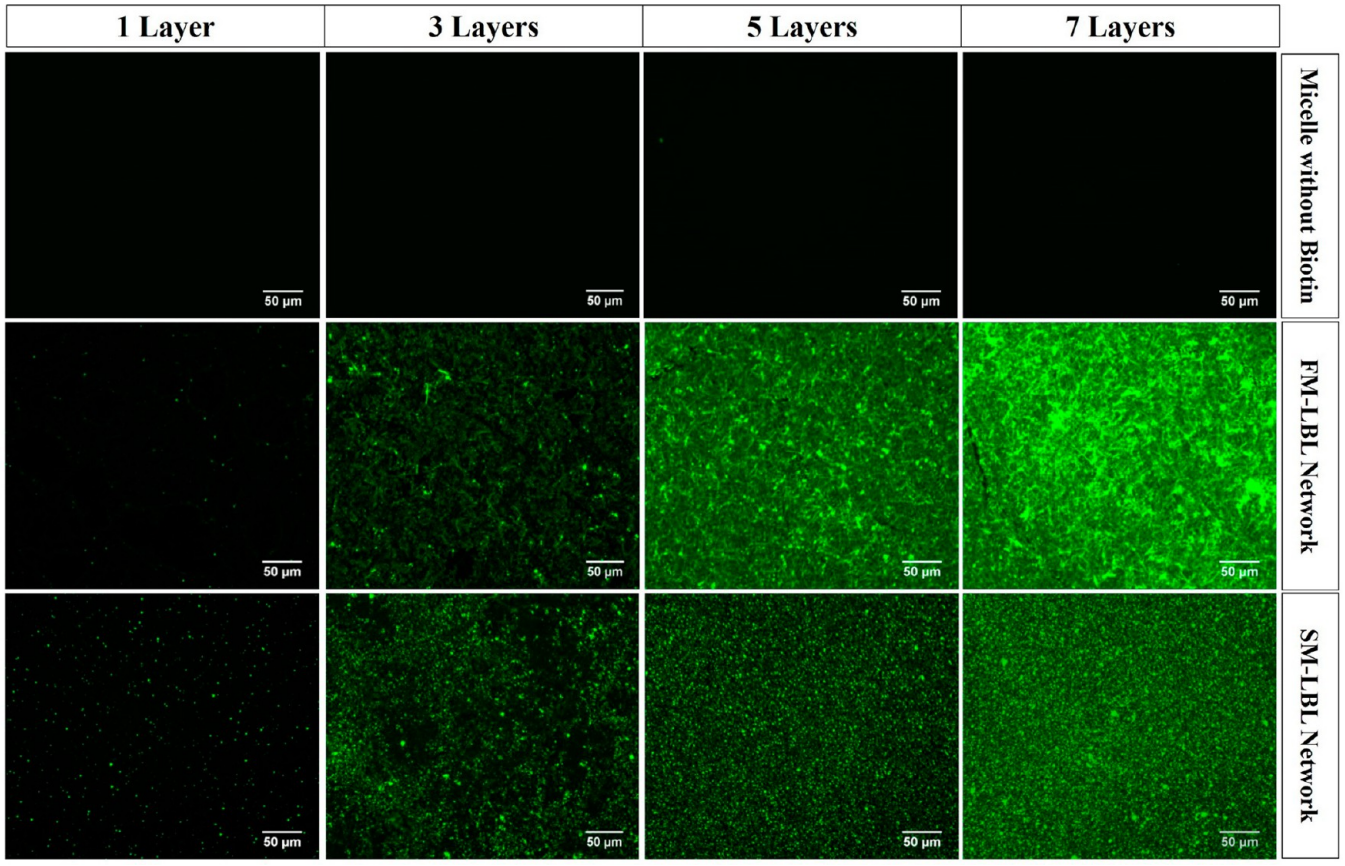

Figure 3. Fluorescence micrographs showing the effect of biotin, micelle morphology (filomicelle (FM) vs spherical micelle (SM)), and number of layer addition cycles (NoL) performed during micelle-LBL network formation on polystyrene substrates.

$$\%\text{bacterial growth} = \frac{(\text{Abs}_{\text{LBL(bacteria)}} - \text{Abs}_{\text{LBL(no-bacteria)}})}{(\text{Abs}_{\text{substrate(bacteria)}} - \text{Abs}_{\text{substrate(no-bacteria}})} \times 100$$

Planktonic Minimum Inhibitory Concentration (MIC) Assay for Free Curcumin. From curcumin stock in DMSO, serial dilutions were made and added to 48 well plates (Thermo Scientific BioLite well plates), with the total DMSO content kept constant at 5% v/v. Then, an overnight culture of *S. aureus* was diluted using BHI medium and added to the well plate curcumin solutions to give 10^5 cell forming units (CFU)/well. At this point, the initial time point (T_0) was recorded at OD_{600} (Molecular Devices Spectramax M2). After 24 h of incubation at 37 °C under orbital shaking (Thermo Scientific REVCO), the final time point (T_f) was recorded at OD_{600}.

RESULTS AND DISCUSSION

Formulating Biotin-Functionalized Polymeric Micelles. Spherical micelles (SM) and filamentous micelles (FM) were synthesized using amphiphilic diblock copolymers of poly(ethylene glycol)-*b*-poly(lactic acid) (PEG-*b*-PLA) via a cosolvent/evaporation method (Figure 1a).[27] See Supporting Information and Figure S1 for diblock copolymer synthesis and characterization. During micelle synthesis (Figure 1a), the progressive evaporation of the dispersed organic phase at the oil/water interface reduces the interfacial tension and increases polymer concentration within the evaporating droplet, resulting in a directed self-assembly of the diblock copolymers.[19,31] As shown in previous studies,[3,18,32] by tuning the copolymer amphiphilicity via the relative hydrophobic block length within methoxy-PEG-PLA (mPEG-PLA), its hydrophobic core packing property is altered to yield different micellar morphologies (Figure 1b). Biotinylated-PEG-PLA was blended with mPEG-PLA to add affinity to the synthesized micelles (see Supporting Information and Figure S2 for synthesis and characterization of biotin-PEG-PLA).

The synthesized micelles were characterized using scanning electron microscopy (SEM) and fluorescence microscopy using curcumin or nile red loaded into the hydrophobic micelles (Figure 1c and Figure S3 in Supporting Information). The mPEG-PLA diblocks with higher PLA content of ∼68−80% w/w formed FM, whereas lower PLA content in the diblocks (PLA < 68% w/w) formed SM, consistent with previously published data.[3,18,33] For all subsequent studies, mPEG5k-PLA50k copolymer was used to form FM, and mPEG5k-PLA20k was used to form SM.

Layer-by-Layer Networks of Micelle. The formulated SM and FM were assembled into 3D porous networks on substrates via a layer-by-layer process involving alternating deposition of streptavidin and either one of the biotinylated micelles driven by specific biotin−streptavidin interactions (scheme shown in Figure 2a). In our current approach, to develop multilayers via oral rinses and to withstand harsh intraoral dynamics (e.g., mechanical (abrasive) and chemical forces), postmolecular self-assembling may require use of multiple forces of molecular interactions. Thus, to improve structural integrity of synthetic mucin networks, strong affinity pairing (e.g., antigen−antibody or biotin−streptavidin) was preferred over conventional charge-based interaction.[34,35] During LBL deposition, the observed increase in fluorescence with number of layer additions (NoL = 1, 3, 5, and 7) demonstrates the ability to grow micelle-LBL networks on

dx.doi.org/10.1021/bm5006917 | *Biomacromolecules* 2014, 15, 3099−3111

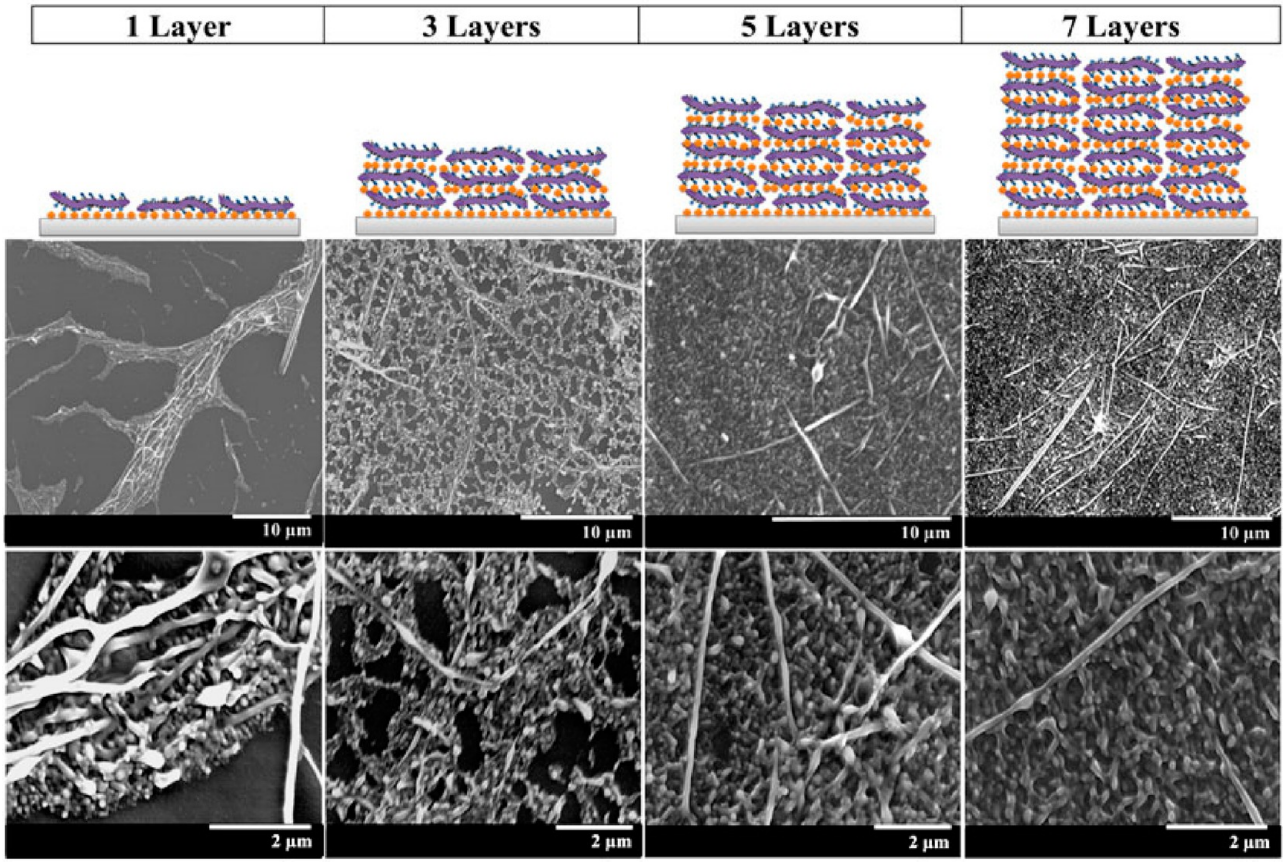

Figure 4. Scanning electron micrographs of micelle-LBL networks made with biotinylated-filomicelles (biotin-FM), illustrating the formation of 3-dimensional porous structures with excellent surface coverage and homogeneity.

surfaces in a regular and predictable fashion. Micelles without biotin were unable to form these multilayered systems because of a lack of specific affinity interactions. Similarly, without streptavidin additions, the biotinylated-micelles cannot effectively cross-link, preventing network growth (see Supporting Information and Figures S6 and S7).

Interestingly, the FM demonstrated an enhanced capacity to self-assemble and form 3D networks compared to the SM, an indication of shape-dependency on network formation (Figure 2b). FM possess an extremely high projected surface area owing to their high structural aspect ratio compared to SM. Aspect ratios $(L/D)_{FM}$ are typically >20 compared to $(L/D)_{SM}$ of ∼1, where L = longer aspect (length) and D = shorter aspect (diameter) (Figure 1c). Thus, FM generates higher ligand−receptor surface interactions during the LBL deposition process, which increase their ability to form networks. Further, the micelle-LBL network initially forms as localized zones of self-assembled clusters (islands) that progressively spreads out to form a continuous network at higher number of layers (Figures 3, 4, 5, and 6a). FMs can span much longer distances with their higher structural aspect ratio, thus permitting easier island bridging and more rapid network development. Therefore, FM-LBL networks self-assembled with at least a 2-fold increase in fluorescence compared to SM-LBL networks at the same number of layers.

In many of the conventional multilayer systems (e.g., inorganic platelets, polyelectrolytes),[36,37] the layer-by-layer process proceeds by forming homogeneous (at the nanoscale) monolayers with each deposition cycle, commonly referred to as normal growth mode. However, in colloidal or nanoparticulate-based systems, the self-assembly growth resulted from localized particulate clusters instead of monolayer deposition. In such systems, multilayers expand via lateral and vertical growth and is more commonly referred to as lateral expansion mode.[36,38,39] A similar network growth pattern was observed in the polymeric micelle based LBL systems. The multivalent polyelectrolyte based systems are structurally more comparable to the biotin-decorated filamentous micelles than the spherical micelles. This structural similarity of the filomicelles is expected to have critically contributed in improving its lateral expansion growth pattern, which was observable with its relatively better substrate coverage and its network formation ability. Interestingly, the network formation mechanism of the filomicelles is strikingly similar to oral salivary mechanisms, suggesting the importance of the filamentous structure to natural mucin subunits, that is, mucin glycoproteins. In a recent study by Baek et al., dental pellicle (enamel-mucin coatings) formation over tooth surfaces was shown to develop through initial "island" like structures composed of oral salivary proteins and associated glycoprotein (mucin) deposition.[40] Over time, these islands would bridge through intermolecular complexation into a continuous film. The dental pellicle protects teeth from demineralization from acid attack.[40,41]

To demonstrate the ability to form FM-LBL networks on biological tissues, networks were deposited ex vivo on excised rat dermal tissue. Again, biotinylated-FM showed a significantly better ability to form LBL networks, whereas FM without biotin (control) showed only a weak increase in fluorescence from nonspecific tissue adsorption. Thus, seven-layered

dx.doi.org/10.1021/bm5006917 | *Biomacromolecules* 2014, 15, 3099−3111

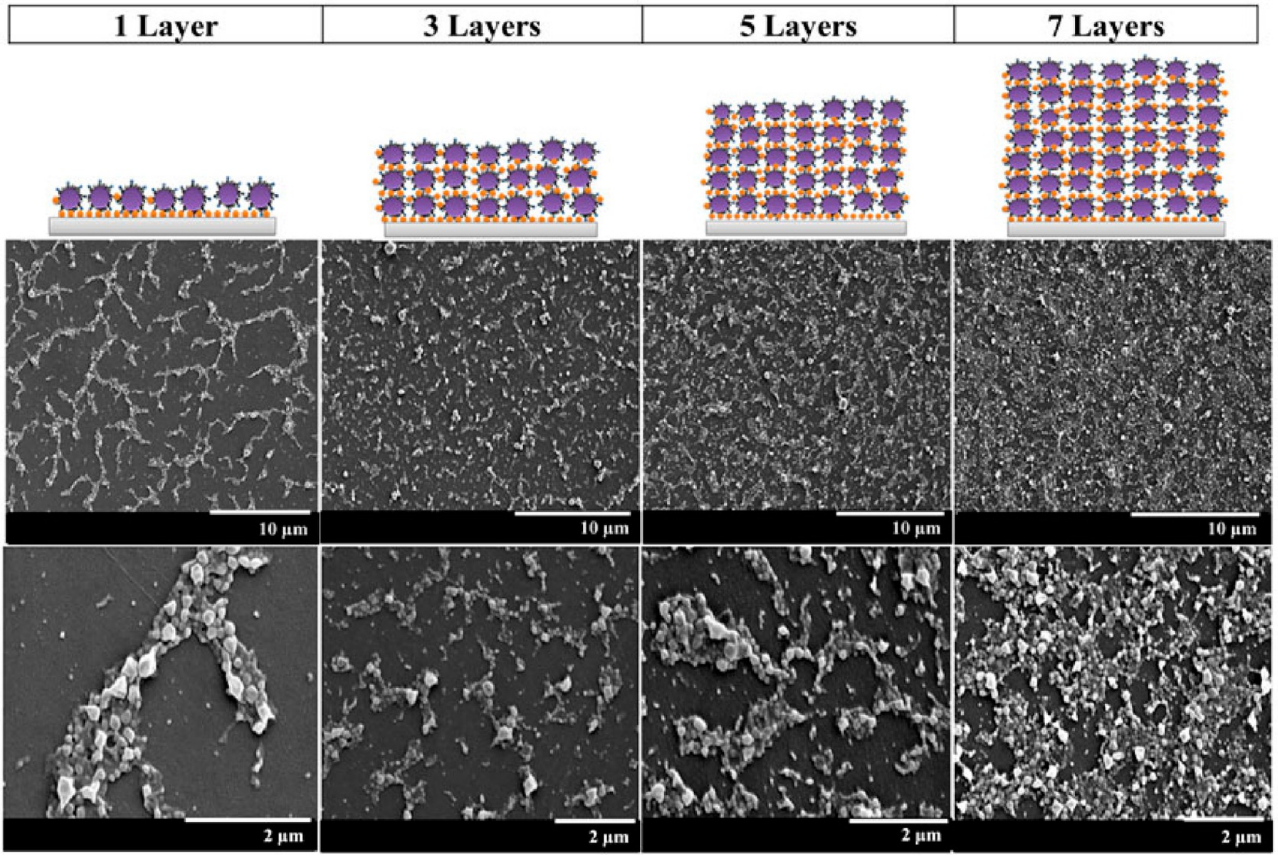

Figure 5. Scanning electron micrographs of micelle-LBL networks made with biotinylated-spherical micelles (biotin-SM), illustrating networks with poor surface coverage and heterogeneity.

biotinylated-FM-LBL networks showed ~2.5-fold higher fluorescence than control FM, conforming the ability to develop FM-LBL networks on tissue surfaces (Figure 2c).

Further, biomolecules (e.g., growth factor, small molecule drugs, and enzymes) can be incorporated into the micellar (FM or SM) cores to render desired bioactivity from the micelle-LBL networks. Also, the degree of network-cross-linking can be altered by controlling the level of biotin that is decorated over micelles during the biotin-micelle synthesis. With high levels of biotin decoration, a more robust network with high network cross-linking and low porosity was expected.[42] Among polymeric micelles, FM possess better shape aspect ratio (L/D) and are structurally analogous to the mucin glycoprotein. Thus, it was expected that filamentous micelles would develop into the desired biomimetic mucin coating and also to serve as an experimental tool for studying structure−function relationships of natural mucin.

Micelle-LBL network properties can also be tailored for different applications by incorporating functional moieties in the synthesized micelles through post modification methods (e.g., chemical modification via covalent coupling). For instance, byssal threads produced by mussels are rich in dihydroxyphenylalanine (DOPA) moiety, the main contributor for their property of strong adhesion. By chemically grafting DOPA molecules with polymeric micelle chains, the networks would be expected to possess superior adhesive property and enhanced film stability.[43,44] Those films can be applied as a robust implant coating capable of drug release.[44] Similarly, charge properties of the network can be altered with careful selection of building blocks, which may impact bacterial adhesion.

Visualizing Homogeneity of the Micelle-LBL Network Coverage and Thickness. Since micelle-LBL networks grew via lateral and vertical expansion, in order to compare apparent network pore size and lateral substrate growth, SM-LBL and FM-LBL networks were visualized using fluorescence microscopy and SEM. In the case of FM-LBL networks, the percent substrate coverage progressively increased with each micelle layer additions (NoL $\leq$ 3) and achieved a near complete coverage for NoL > 3 (Figures 3, 4, and 6a). This increasing coverage with NoL illustrates the networks lateral growth expansion. Interestingly, the FM-LBL networks with higher NoL demonstrated formation of a nanoporous network with an average pore diameter of ~110 to 340 nm under SEM (Figure 7c). In literature,[45] the average mesh size in natural mucin-networks (cervical) was reported to range between 20 and 200 nm with an average pore size of ~100 nm, this closely matches with synthetic networks.

Unlike FM-LBL networks, the SM-LBL networks resulted in inhomogeneous substrate coverage (Figures 3 and 5) and would probably require a much higher NoL (>7) to achieve complete coverage. The improved coverage by the FM-LBL networks was visually evident under both fluorescence microscopy and SEM, where it was deduced that five-layer additions resulted in ~100% coverage, whereas SM-LBL networks achieved only ~38% coverage (Figure 6b). Thickness measurements of the more homogeneous FM-LBL network using confocal laser scanning microscopy (CLSM) showed a linear growth with increasing number of layer (Figure 7a,b),

dx.doi.org/10.1021/bm5006917 | *Biomacromolecules* 2014, 15, 3099−3111

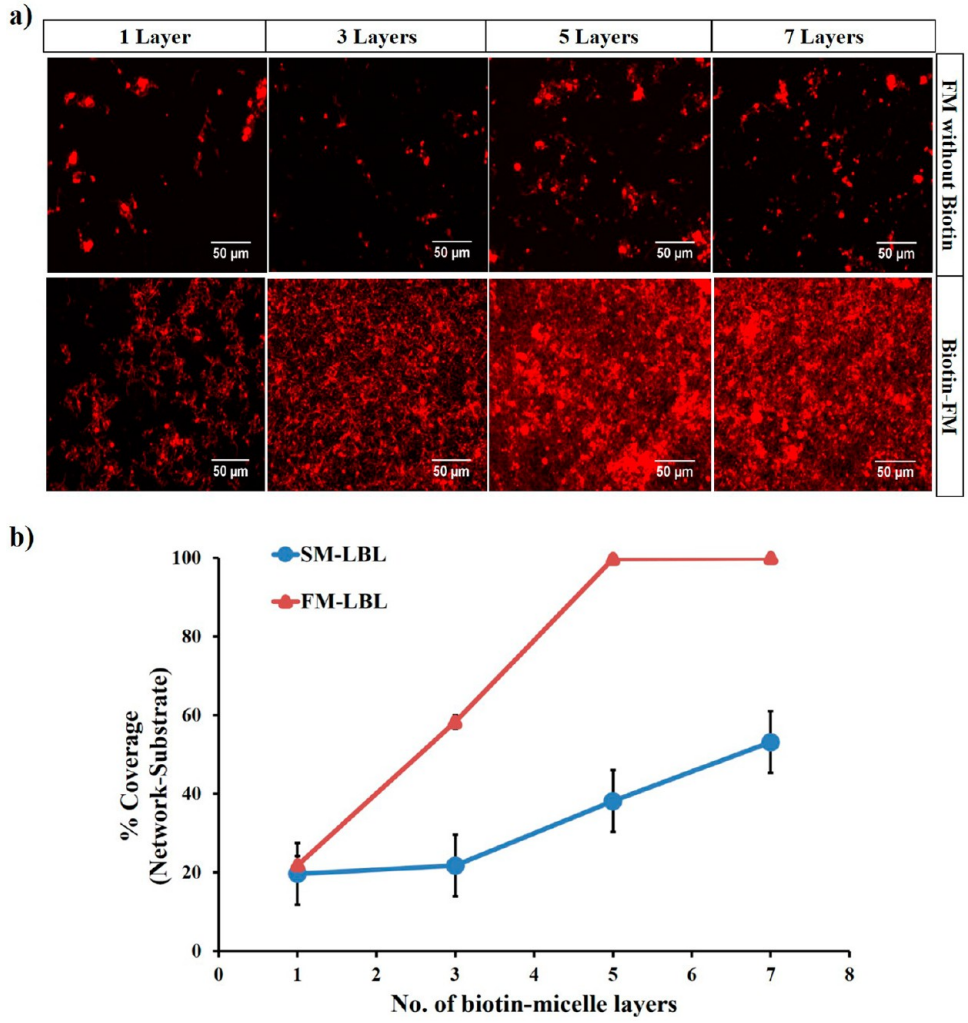

Figure 6. (a) Fluorescence micrographs of micelle-LBL networks made with nile red-loaded filomicelles corroborate the network formation trends observed with curcumin-loaded filomicelles (see Figure 3). (b) Percent substrate coverage by the filomicelle (FM) and spherical micelle (SM)-LBL networks. FM-LBL networks provided complete surface coverage, whereas SM-LBL networks showed a significantly lower surface coverage for same number of layer additions (NoL). Percent surface coverage was deduced from ImageJ postprocessing, where network coverage and unoccupied substrate surface area at different levels of magnification was obtained.

where networks with seven-layer additions were ∼4 μm thick. The growth in total network thickness serves as an illustration of networks vertical growth expansion. Interestingly, the thickness of natural mucin networks vary from 70 to 1000 μm, depending on the region within oral cavity.[46,47] Structurally, mucin multilayers possess loosely held outer layers that are prone to bacterial colonization and are constantly subjected to dynamic removal and reformation. This contrasts with the more structurally intact epithelial-bound innermost layer that is devoid of bacteria.[48−50] Transitioning the current approach from micro- to mesoscopic length scale may require a higher number of oral rinse cycles or, more feasibly, incorporation of simple modifications in the preassembly structures (e.g., inclusion of hydrating polymers). Therefore, by ensuring network stability in synthetic mucin networks, they can serve as an effective model to structurally recreate the more firmly held mucosal adjoining layers.

Chemical Stability of FM-LBL Networks. In the oral environment, the micelle-LBL networks are exposed to both salivary fluid and bacterial proteases. Bacterial colonization in the oral cavity produces a highly proteolytic environment causing the natural mucin to transition into a more loosely held network. These result from cleavage of the intermolecular protein linkages, causing a more rapid mucin removal (peel-out).[48] Therefore, to assess the durability of the LBL networks against the chemical onslaughts, seven-layered FM-LBL networks were deposited on polystyrene (PS) substrates, and subjected to network destabilization in bacterial proteolytic enzyme (pronase) and in simulated saliva. The FM-LBL network stability was monitored by independently quantifying streptavidin loss from the innermost streptavidin layer and from the overlaying network layers (scheme shown in Figure 8).

In our previous work,[51] we showed that the base streptavidin layer without any overlaying micelle-LBL network destabilizes rapidly upon direct protease exposure, resulting in ∼90% loss (after ∼42 h). However, when a micelle-LBL network was developed over this base layer, it functioned as a protective barrier to shield the innermost streptavidin layer from destabilization. We observed that nearly 45% of the streptavidin mass remained (for ∼44 h) in the networks without being destabilized by the harsh protease (Figure 8).

dx.doi.org/10.1021/bm5006917 | Biomacromolecules 2014, 15, 3099−3111

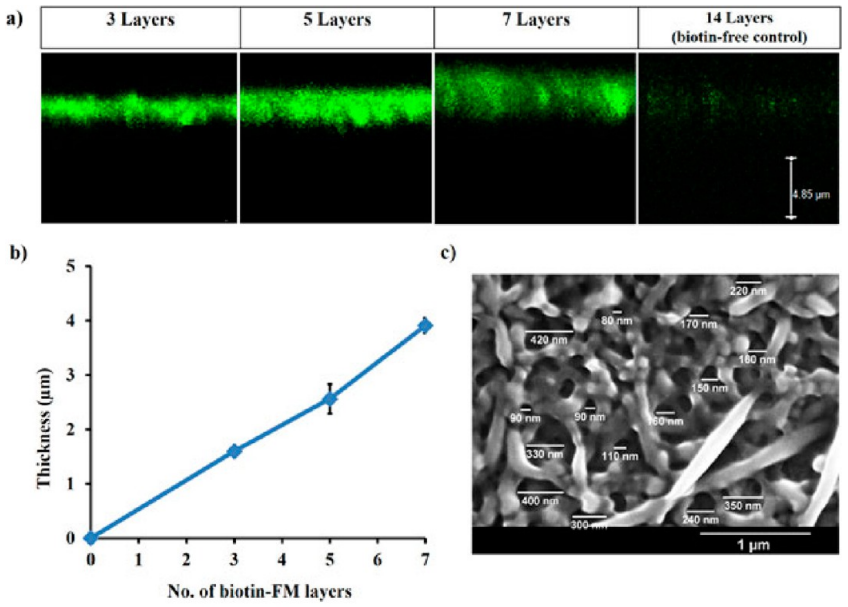

Figure 7. (a, b) Thickness measurement of FM-LBL networks. Network thickness measurements from fluorescence image stacks obtained using confocal laser scanning microscopy (CLSM) demonstrate a linear increase in thickness with number of layers, where a seven-layered micelle-LBL self-assembly showed an ~4 μm thick network. (CLSM imaging measurement parameters: 63× water immersion objective, *xzy* scanning mode with *y*-stacking, scan size width (x) × height (y) × depth (z) = 110 × 110 (50–60) μm, No. of optical sections = 46–65). (c) Seven-layered FM-LBL networks demonstrated formation of a nanoporous network of average pore diameter of ~110–340 nm under SEM.

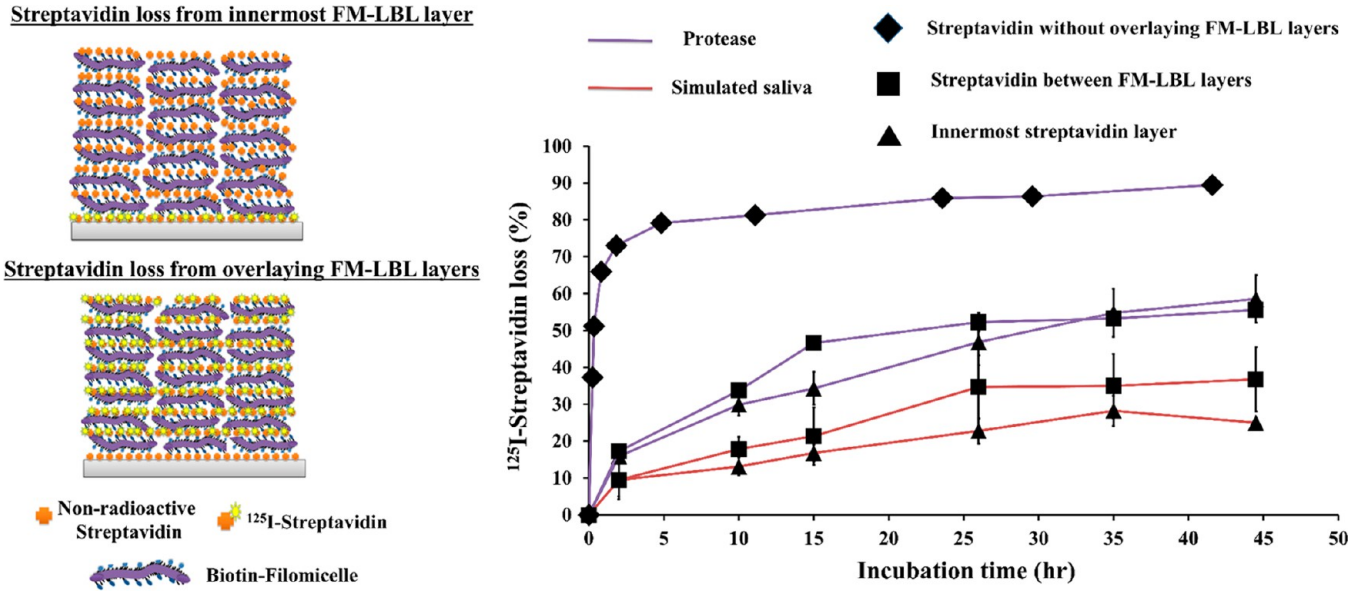

Figure 8. In vitro chemical stability of FM-LBL networks under simulated oral environment. Destabilization of innermost streptavidin layer and overlaying streptavidin layers was tracked independently to study overall network stability under simulated salivary and protease environment.

Expectedly, the proteolytic enzyme, pronase, possesses relatively higher destabilization effect on the protein cross-linked LBL networks than the simulated saliva. The innermost streptavidin layer loss was nearly 56% less (after ~2 days) under simulated saliva than in pronase. A similar effect was observed on the streptavidin in the overlaying micelle layers, where the loss was nearly 39% lower (after ~2 days) under simulated saliva.

Interestingly, streptavidin removal from the innermost and the overlaying FM-LBL network layers showed only moderate reduction, with insignificant differences between the two locations. This suggests accessibility of the innermost layers of the FM-LBL networks to the proteolytic enzyme. This level of accessibility can be attributed to the porosity of the LBL network akin to that of natural mucin.

Wettability Studies. In the mucin networks, the hydrophilic protein domains are exposed to outer environment to yield a hydrated surface.[52,53] In patients suffering from loss of the mucin barrier, surface hydration is poor with reduced wettability. To study the degree of wettability of our synthetic mucin, FM-LBL networks with different NoL (1, 3, 5, and 7) were developed on PS substrates. As expected, the unmodified hydrophobic PS substrate showed a high water contact angle (~90°), demonstrating poor wettability. However, as the

dx.doi.org/10.1021/bm5006917 | *Biomacromolecules* 2014, 15, 3099–3111

synthetic mucin (FM-LBL) network was self-assembled over the substrate, a significant reduction in contact angle was observed, confirming wettability. The contact angle progressively decreased to 34.5° with an increase in NoL from 1 to 3, indicating that the progressive increase in surface coverage impacted wettability. These observations are congruent with our earlier observations with SEM and fluorescence microscopy imaging where networks with NoL $\leq$ 3 layers achieved incomplete surface coverage, though coverage increased with number of layer additions (Figure 6b). Beyond three micelle layer additions (NoL $\geq$ 5), FM-LBL networks achieved near complete substrate coverage, yielding a consistently low contact angle of 29° (Figure S4 in Supporting Information). The high wettability of FM-LBL networks is due to hydrophilic contributions from the exposed PEG micellar chains and hydrophilic domains of the protein streptavidin.

Bacterial Growth Studies. Natural oral mucin alters the growth of microbial flora, permitting adherence and proliferation of certain microbes while also acting as a clearing agent.[12] As described earlier, the outer layers of mucin networks are less structurally intact and form an expanded volume.[48] These outer mucin layers are prone to bacterial colonization and subsequently function as a sacrificial barrier. Such a mucin coat when coupled with persistent salivary flow reduces oral bacterial residence time to deter undesirable biofilm formation.[54] In patients lacking the protective mucin barrier, there is an increased susceptibility to excessive bacterial colonization and biofilm formation leading to oral infections.[55−57]

FM-LBL networks promoted adhesion of *S. aureus* bacteria compared to SM-LBL networks, most likely due to higher surface area availability and network porosity. On the other hand, the inhomogeneous SM-LBL networks did not significantly alter bacterial growth compared to control substrates without any LBL networks (Figure 9a). Interestingly, such enhanced bacterial adhesion on FM-LBL networks would be typically unexpected for a network system composed of PEG, which is well-known for its antiadhesion properties. This outcome highlights a critical biomimetic property of the FM-LBL networks in that they support bacterial growth by recreating the morphology and function of natural mucin.[58,59]

Another advantage of the FM-LBL network is its ability to serve as a drug delivery vehicle. This may be useful as an alternative method to control bacterial growth, in particular, when unhealthy infections need to be controlled. To demonstrate this ability, LBL networks were created using curcumin-loaded SM and FM. Curcumin is a natural antioxidant with known antimicrobial properties.[60] The curcumin-loaded FM-LBL networks resulted in ~31% reduction in bacterial growth, whereas the relatively less homogeneous curcumin-loaded SM-LBL networks did not significantly reduce bacterial adherence (Figure 9b). Again, this can be attributed to the poor network formation of SM-LBL network that resulted in lower drug content and insignificant effects on bacteria. FM-LBL networks with better self-assembly and, thereby, increased drug content thus resulted in a reduced bacterial growth.

Additional control layer-by-layer networks of spherical and filamentous micelles were also studied independently without bacterial addition to account for nonspecific crystal violet staining of the micelles. Any nonspecific micelle staining was accounted for in the bacterial growth (%) calculations (see Supporting Information and Figure S8). To corroborate the effect of curcumin on inhibiting bacterial growth, the results

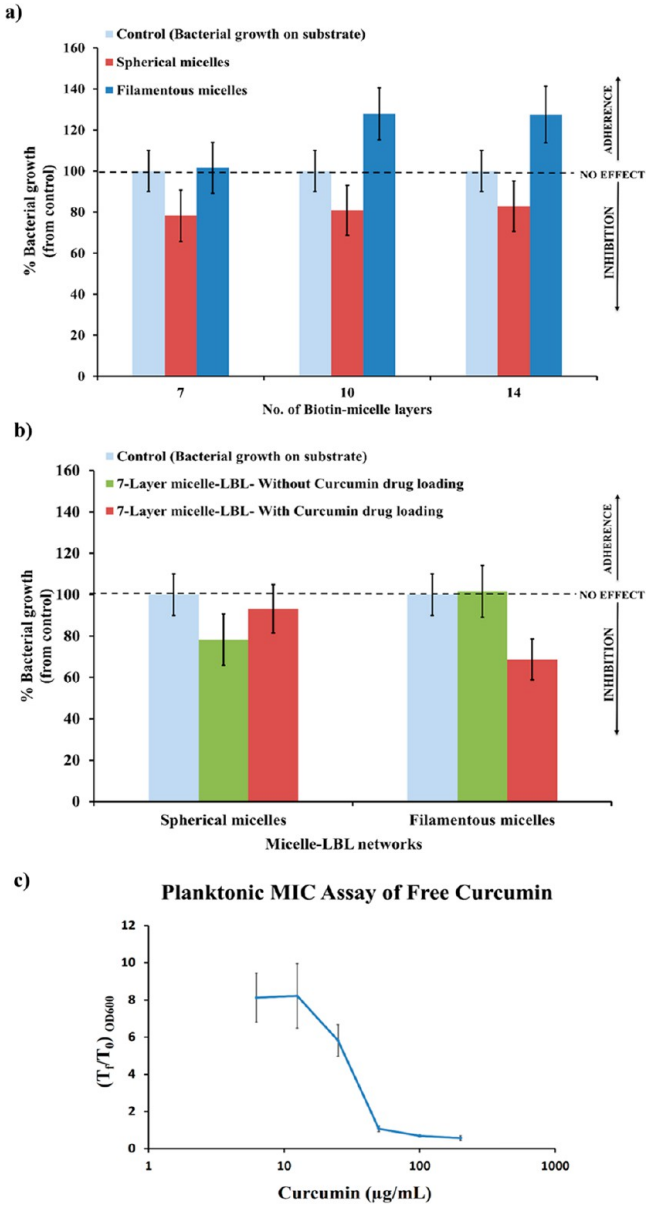

Figure 9. Bacterial growth on micelle-LBL networks measured using crystal violet stain, after treatment duration of ~24 h. Additional control measurements were performed to account for nonspecific crystal violet staining of micelles without bacterial growth (see Supporting Information and Figure S8). (a) Bacterial growth on FM-LBL and SM-LBL networks with increasing number of layer additions (7, 10, and 14) were developed using micelles without curcumin loading. Bacterial growth was significantly higher on FM-LBL networks than the SM-LBL networks (NoL = 10 and 14), which is likely due to increased surface area available for bacterial growth. (b) Effect of curcumin loading in micelles on suppressing bacterial growth on seven-layered SM-LBL and FM-LBL networks. A reduction in bacterial growth was observed on curcumin-loaded FM-LBL networks, indicative of curcumin antibacterial activity. (c) Planktonic minimum inhibitory concentration (MIC) assay for free curcumin. Optical density, OD_{600} at initial time point (T_0) and after 24 h incubation (T_f) was recorded and used in studying the extent of planktonic inhibition at different free curcumin concentrations.

from micelle-LBL networks were compared to the planktonic antimicrobial activity of free curcumin. The minimum inhibitory concentration required to suppress 90% bacterial *S. aureus* growth (MIC_{90}) was found to be ~50 μg/mL for free

dx.doi.org/10.1021/bm5006917 | *Biomacromolecules* 2014, 15, 3099−3111

curcumin, which indicates a strong antimicrobial effect (Figure 9c). FM-LBL and SM-LBL networks were expected to yield a curcumin solution concentration of ~24.5 and ~7.5 μg/mL, respectively, at 24 h drug release. Based on the planktonic MIC_{90} plot, these concentrations were expected to inhibit ~31.5 and ~0% bacterial growth for FM-LBL and SM-LBL, respectively. Effects of released curcumin were comparable with those observed from the inhibition study with bacteria seeded directly on curcumin-loaded micelle-LBL networks, confirming the antibacterial role played by curcumin.

CONCLUSIONS

FM-LBL networks can be developed to recreate the structural properties of oral mucin barriers. The tunable characteristics of these networks open up a range of potential applications and studies that are not currently possible with other analog systems. The developed synthetic mucin network possessed excellent surface hydration property and remained stable under harsh proteolytic and salivary environments. Further, incorporation of a suitable antibacterial drug within the network provides a way to control bacterial growth and inhibit undesirable biofilm formation. Thus, such bioactive interfaces that structurally and functionally mimic the natural mucin barrier, present exciting opportunities for oral drug delivery and regenerative medicine.

ASSOCIATED CONTENT

Supporting Information

Contains information on synthesis and characterization of amphiphilic PEG-PLA based diblock copolymers (Figures S1 and S2); nile red-loaded filomicelles visualization (Figure S3); sessile drop-contact angle measurements on FM-LBL networks to evaluate its surface hydration properties (Figure S4); confocal laser scanning micrographs of curcumin-loaded FM-LBL networks showing network structures (Figure S5); procedure for radiolabeling streptavidin; evaluating extent of nonspecific LBL growth from biotin-micelle depositions without complementary streptavidin additions (Figures S6 and S7); evaluation of nonspecific crystal violet staining on micelle-LBL networks (Figure S8). This material is available free of charge via the Internet at http://pubs.acs.org.

AUTHOR INFORMATION

Corresponding Author

*E-mail: dziubla@engr.uky.edu.

Present Address

‡Bluegrass Advanced Materials, LLC, A268 ASTeCC, Lexington, KY 40506.

Notes

The authors declare no competing financial interest.

ACKNOWLEDGMENTS

This work was funded by National Institutes of Health (Grant R03 DE019496). Authors would like to acknowledge James G. Begley and Cindy Meier for performing confocal laser scanning measurements, and Dr. Bradley Berron and Leila Safazadeh for their help with the goniometer-contact angle measurements. Authors also thank Dr. Paritosh Wattamwar for insightful discussions.

ABBREVIATIONS

AFM, atomic force microscopy; BHI, brain heart infusion; biotin-FM, biotinylated-filomicelles; biotin-PEG-PLA, biotinylated-poly(ethylene glycol)-*b*-poly(lactic acid); biotin-SM, biotinylated-spherical micelles; CFU, cell forming units; CLSM, confocal laser scanning microscopy; DCC, *N*,*N*′-dicyclohexylcarbodiimide; DCM, dichloromethane; DMSO, dimethyl sulfoxide; DOPA, dihydroxyphenylalanine; FM, filamentous micelles; FM-LBL, layer-by-layer networks of filomicelles; FTIR, Fourier transform infrared spectroscopy; GPC, gel permeation chromatography; LBL, layer-by-layer; MIC, minimum inhibitory concentration; micelle-LBL, layer-by-layer networks of micelles; mPEG, methoxy-poly(ethylene glycol); mPEG-PLA, methoxy-poly(ethylene glycol)-*b*-poly(lactic acid); mPEG5k-PLA20k, mPEG (MW ~5000 Da)-PLA (MW ~ 20 000 Da); mPEG5k-PLA50k, mPEG (MW ~ 5000 Da)-PLA (MW ~ 50000 Da); NoL, number of layer additions; OD, optical density; PEG, poly(ethylene glycol); PEG-*b*-PLA, poly(ethylene glycol)-*block*-poly(lactic acid) copolymer; PLA, poly(lactic acid); PS, polystyrene; ^{1}H NMR, proton nuclear magnetic resonance; RFU, Relative fluorescence intensity; ROP, Ring opening polymerization; SEM, scanning electron microscopy; SM, spherical micelles; SM-LBL, layer-by-layer networks of spherical micelles

REFERENCES

(1) Kim, Y.; Dalhaimer, P.; Christian, D. A.; Discher, D. E. Polymeric worm micelles as nano-carriers for drug delivery. *Nanotechnology* **2005**, *16* (7), S484−91.

(2) Kaditi, E.; Mountrichas, G.; Pispas, S.; Demetzos, C. Block copolymers for drug delivery nano systems (DDnSs). *Curr. Med. Chem.* **2012**, *19* (29), 5088−100.

(3) Simone, E. A.; Dziubla, T. D.; Colon-Gonzalez, F.; Discher, D. E.; Muzykantov, V. R. Effect of polymer amphiphilicity on loading of a therapeutic enzyme onto protective fulamentous and spherical polymer nanocarrlers. *Biomacromolecules* **2007**, *8* (12), 3914−3921.

(4) Ott, C.; Hoogenboom, R.; Hoeppener, S.; Wouters, D.; Gohy, J.-F.; Schubert, U. S. Tuning the morphologies of amphiphilic metallo-supramolecular triblock terpolymers: from spherical micelles to switchable vesicles. *Soft Matter* **2009**, *5* (1), 84−91.

(5) Groschel, A. H.; Schacher, F. H.; Schmalz, H.; Borisov, O. V.; Zhulina, E. B.; Walther, A.; Muller, A. H. E. Precise hierarchical self-assembly of multicompartment micelles. *Nat. Commun.* **2012**, 3.

(6) Qiu, H.; Russo, G.; Rupar, P. A.; Chabanne, L.; Winnik, M. A.; Manners, I. Tunable supermicelle architectures from the hierarchical self-assembly of amphiphilic cylindrical B-A-B triblock co-micelles. *Angew. Chem.* **2012**, *51* (47), 11882−5.

(7) Zhu, Z.; Gao, N.; Wang, H.; Sukhishvili, S. A. Temperature-triggered on-demand drug release enabled by hydrogen-bonded multilayers of block copolymer micelles. *J. Controlled Release* **2013**, *171* (1), 73−80.

(8) Matsuzawa, A.; Matsusaki, M.; Akashi, M. Effectiveness of nanometer-sized extracellular matrix layer-by-layer assembled films for a cell membrane coating protecting cells from physical stress. *Langmuir* **2013**, *29* (24), 7362−7368.

(9) Chung, W. J.; Oh, J. W.; Kwak, K.; Lee, B. Y.; Meyer, J.; Wang, E.; Hexemer, A.; Lee, S. W. Biomimetic self-templating supramolecular structures. *Nature* **2011**, *478* (7369), 364−8.

(10) O'Leary, L. E.; Fallas, J. A.; Bakota, E. L.; Kang, M. K.; Hartgerink, J. D. Multi-hierarchical self-assembly of a collagen mimetic peptide from triple helix to nanofibre and hydrogel. *Nat. Chem.* **2011**, *3* (10), 821−8.

(11) Roussel, P.; Lamblin, G.; Lhermitte, M.; Houdret, N.; Lafitte, J. J.; Perini, J. M.; Klein, A.; Scharfman, A. The complexity of mucins. *Biochimie* **1988**, *70* (11), 1471−82.

(12) Tabak, L. A.; Levine, M. J.; Mandel, I. D.; Ellison, S. A. Role of salivary mucins in the protection of the oral cavity. *J. Oral Pathol. Med.* **1982**, *11* (1), 1−17.
(13) Cone, R. A. Barrier properties of mucus. *Adv. Drug Delivery Rev.* **2009**, *61* (2), 75−85.
(14) Sheehan, J. K.; Thornton, D. J.; Somerville, M.; Carlstedt, I. Mucin structure. The structure and heterogeneity of respiratory mucus glycoproteins. *Am. Rev. Respir. Dis.* **1991**, *144* (3 Pt 2), S4−9.
(15) Bansil, R.; Turner, B. S. Mucin structure, aggregation, physiological functions and biomedical applications. *Curr. Opin. Colloid Interface Sci.* **2006**, *11* (2−3), 164−170.
(16) Thornton, D. J.; Khan, N.; Mehrotra, R.; Howard, M.; Veerman, E.; Packer, N. H.; Sheehan, J. K. Salivary mucin MG1 is comprised almost entirely of different glycosylated forms of the MUC5B gene product. *Glycobiology* **1999**, *9* (3), 293−302.
(17) Visvanathan, V.; Nix, P. Managing the patient presenting with xerostomia: a review. *Int. J. Clin. Pract.* **2010**, *64* (3), 404−7.
(18) Simone, E. A.; Dziubla, T. D.; Arguiri, E.; Vardon, V.; Shuvaev, V. V.; Christofidou-Solomidou, M.; Muzykantov, V. R. Loading PEG-catalase into filamentous and spherical polymer nanocarriers. *Pharm. Res.* **2009**, *26* (1), 250−260.
(19) Zhu, J. T.; Ferrer, N.; Hayward, R. C. Tuning the assembly of amphiphilic block copolymers through instabilities of solvent/water interfaces in the presence of aqueous surfactants. *Soft Matter* **2009**, *5* (12), 2471−2478.
(20) Crater, J. S.; Carrier, R. L. Barrier properties of gastrointestinal mucus to nanoparticle transport. *Macromol. Biosci.* **2010**, *10* (12), 1473−83.
(21) Lieleg, O.; Vladescu, I.; Ribbeck, K. Characterization of particle translocation through mucin hydrogels. *Biophys. J.* **2010**, *98* (9), 1782−9.
(22) Critchfield, A. S.; Yao, G.; Jaishankar, A.; Friedlander, R. S.; Lieleg, O.; Doyle, P. S.; McKinley, G.; House, M.; Ribbeck, K. Cervical mucus properties stratify risk for preterm birth. *PloS One* **2013**, *8* (8), e69528.
(23) Lai, S. K.; Wang, Y. Y.; Cone, R.; Wirtz, D.; Hanes, J. Altering mucus rheology to "solidify" human mucus at the nanoscale. *PloS One* **2009**, *4* (1), e4294.
(24) Nordgard, C. T.; Nonstad, U.; Olderoy, M. O.; Espevik, T.; Draget, K. I. Alterations in mucus barrier function and matrix structure induced by guluronate oligomers. *Biomacromolecules* **2014**, *15* (6), 2294−300.
(25) Hong, Z. N.; Chasan, B.; Bansil, R.; Turner, B. S.; Bhaskar, K. R.; Afdhal, N. H. Atomic force microscopy reveals aggregation of gastric mucin at low pH. *Biomacromolecules* **2005**, *6* (6), 3458−3466.
(26) Kirch, J.; Schneider, A.; Abou, B.; Hopf, A.; Schaefer, U. F.; Schneider, M.; Schall, C.; Wagner, C.; Lehr, C. M. Optical tweezers reveal relationship between microstructure and nanoparticle penetration of pulmonary mucus. *Proc. Natl. Acad. Sci. U.S.A.* **2012**, *109* (45), 18355−18360.
(27) Cai, S. S.; Vijayan, K.; Cheng, D.; Lima, E. M.; Discher, D. E. Micelles of different morphologies - Advantages of worm-like filomicelles of PEO-PCL in paclitaxel delivery. *Pharm. Res.* **2007**, *24* (11), 2099−2109.
(28) Zhu, J. T.; Hayward, R. C. Spontaneous generation of amphiphilic block copolymer micelles with multiple morphologies through interfacial instabilities. *J. Am. Chem. Soc.* **2008**, *130* (23), 7496−7502.
(29) Wong, C. F.; Yuen, K. H.; Peh, K. K. An in vitro method for buccal adhesion studies: importance of instrument variables. *Int. J. Pharm.* **1999**, *180* (1), 47−57.
(30) Merritt, J. H.; Kadouri, D. E.; O'Toole, G. A., Growing and analyzing static biofilms. *Curr. Protoc. Microbiol.* **2005**, 10.1002/9780471729259.mc01b01s00.
(31) Zhu, J.; Hayward, R. C. Hierarchically structured microparticles formed by interfacial instabilities of emulsion droplets containing amphiphilic block copolymers. *Angew. Chem., Int. Ed.* **2008**, *47* (11), 2113−2116.
(32) Simone, E. A.; Dziubla, T. D.; Discher, D. E.; Muzykantov, V. R. Filamentous polymer nanocarriers of tunable stiffness that encapsulate the therapeutic enzyme catalase. *Biomacromolecules* **2009**, *10* (6), 1324−1330.
(33) Ahmed, F.; Discher, D. E. Self-porating polymersomes of PEG-PLA and PEG-PCL: hydrolysis-triggered controlled release vesicles. *J. Controlled Release* **2004**, *96* (1), 37−53.
(34) Tang, Z. Y.; Wang, Y.; Podsiadlo, P.; Kotov, N. A. Biomedical applications of layer-by-layer assembly: From biomimetics to tissue engineering. *Adv. Mater.* **2006**, *18*, 3203. *Adv. Mater.* **2007**, *19* (7), 906−906.
(35) Wang, M. J.; Wang, L. Y.; Yuan, H.; Ji, X. H.; Sun, C. Y.; Ma, L.; Bai, Y. B.; Li, T. J.; Li, J. H. Immunosensors based on layer-by-layer self-assembled Au colloidal electrode for the electrochemical detection of antigen. *Electroanalysis* **2004**, *16* (9), 757−764.
(36) Jeon, J.; Panchagnula, V.; Pan, J.; Dobrynin, A. V. Molecular dynamics simulations of multilayer films of polyelectrolytes and nanoparticles. *Langmuir* **2006**, *22* (10), 4629−37.
(37) Kleinfeld, E. R.; Ferguson, G. S. Stepwise formation of multilayered nanostructural films from macromolecular precursors. *Science* **1994**, *265* (5170), 370−373.
(38) Ostrander, J. W.; Mamedov, A. A.; Kotov, N. A. Two modes of linear layer-by-layer growth of nanoparticle-polylectrolyte multilayers and different interactions in the layer-by-layer deposition. *J. Am. Chem. Soc.* **2001**, *123* (6), 1101−1110.
(39) Mohanta, V.; Patil, S. Enhancing surface coverage and growth in layer-by-layer assembly of protein nanoparticles. *Langmuir* **2013**, *29* (43), 13123−13128.
(40) Baek, J. H.; Krasieva, T.; Tang, S.; Ahn, Y.; Kim, C. S.; Vu, D.; Chen, Z.; Wilder-Smith, P. Optical approach to the salivary pellicle. *J. Biomed. Opt.* **2009**, *14* (4), 044001.
(41) Nieuw Amerongen, A. V.; Oderkerk, C. H.; Driessen, A. A. Role of mucins from human whole saliva in the protection of tooth enamel against demineralization in vitro. *Caries Res.* **1987**, *21* (4), 297−309.
(42) Zhao, Y.; Bertrand, J.; Tong, X.; Zhao, Y. Photo-cross-linkable polymer micelles in hydrogen-bonding-built layer-by-layer films. *Langmuir* **2009**, *25* (22), 13151−7.
(43) Wu, J.; Zhang, L.; Wang, Y.; Long, Y.; Gao, H.; Zhang, X.; Zhao, N.; Cai, Y.; Xu, J. Mussel-inspired chemistry for robust and surface-modifiable multilayer films. *Langmuir* **2011**, *27* (22), 13684−91.
(44) Karabulut, E.; Pettersson, T.; Ankerfors, M.; Wagberg, L. Adhesive layer-by-layer films of carboxymethylated cellulose nanofibril-dopamine covalent bioconjugates inspired by marine mussel threads. *ACS Nano* **2012**, *6* (6), 4731−9.
(45) Olmsted, S. S.; Padgett, J. L.; Yudin, A. I.; Whaley, K. J.; Moench, T. R.; Cone, R. A. Diffusion of macromolecules and virus-like particles in human cervical mucus. *Biophys. J.* **2001**, *81* (4), 1930−7.
(46) Collins, L. M.; Dawes, C. The surface area of the adult human mouth and thickness of the salivary film covering the teeth and oral mucosa. *J. Dent. Res.* **1987**, *66* (8), 1300−2.
(47) Tabak, L. A. In defense of the oral cavity: structure, biosynthesis, and function of salivary mucins. *Annu. Rev. Physiol.* **1995**, *57*, 547−64.
(48) Johansson, M. E. V.; Phillipson, M.; Petersson, J.; Velcich, A.; Holm, L.; Hansson, G. C. The inner of the two Muc2 mucin-dependent mucus layers in colon is devoid of bacteria. *Proc. Natl. Acad. Sci. U.S.A.* **2008**, *105* (39), 15064−15069.
(49) Atuma, C.; Strugala, V.; Allen, A.; Holm, L. The adherent gastrointestinal mucus gel layer: thickness and physical state in vivo. *Am. J. Physiol.: Gastrointest. Liver Physiol.* **2001**, *280* (5), G922−9.
(50) Derrien, M.; van Passel, M. W.; van de Bovenkamp, J. H.; Schipper, R. G.; de Vos, W. M.; Dekker, J. Mucin-bacterial interactions in the human oral cavity and digestive tract. *Gut Microbes* **2010**, *1* (4), 254−268.
(51) Authimoolam, S. P.; Puleo, D. A.; Dziubla, T. D. Affinity based multilayered polymeric self-assemblies for oral wound applications. *Adv. Healthcare Mater.* **2013**, *2* (7), 983−92.
(52) Ranc, H.; Elkhyat, A.; Servais, C.; Mac-Mary, S.; Launay, B.; Humbert, P. Friction coefficient and wettability of oral mucosal tissue:

Changes induced by a salivary layer. *Colloids Surf., A* **2006**, *276* (1−3), 155−161.
(53) Shi, L.; Caldwell, K. D. Mucin adsorption to hydrophobic surfaces. *J. Colloid Interface Sci.* **2000**, *224* (2), 372−381.
(54) Melvin, J. E. Saliva and dental diseases. *Curr. Opin. Dent.* **1991**, *1* (6), 795−801.
(55) Turner, M. D.; Ship, J. A. Dry mouth and its effects on the oral health of elderly people. *J. Am. Dent. Assoc.* **2007**, *138*, 15s−20s.
(56) Mese, H.; Matsuo, R. Salivary secretion, taste and hyposalivation. *J. Oral Rehabil.* **2007**, *34* (10), 711−723.
(57) Hopcraft, M. S.; Tan, C., Xerostomia: an update for clinicians. *Aust. Dent. J.* **2010**, *55*, (3), 238−44; quiz 353.
(58) Kingshott, P.; Wei, J.; Bagge-Ravn, D.; Gadegaard, N.; Gram, L. Covalent attachment of poly(ethylene glycol) to surfaces, critical for reducing bacterial adhesion. *Langmuir* **2003**, *19* (17), 6912−6921.
(59) Chen, S. F.; Li, L. Y.; Zhao, C.; Zheng, J. Surface hydration: Principles and applications toward low-fouling/nonfouling biomaterials. *Polymer* **2010**, *51* (23), 5283−5293.
(60) Gunes, H.; Gulen, D.; Mutlu, R.; Gumus, A.; Tas, T.; Eren Topkaya, A. Antibacterial effects of curcumin: an in vitro minimum inhibitory concentration study. *Toxicol. Ind. Health* **2013**, DOI: 10.1186/1472-6882-13-269.